Fracture energy in phase field models

Fracture energy in phase field models

Francesco Freddi*

Department of Engineering and Architecture, University of Parma, Parco Area delle Scienze 181/A, I 43124 Parma

Abstract

The phase field approach to brittle fracture is based on smeared energetic representation of sharp fracture into surface. The passage between damaged and undamaged zones is influenced by an internal length scale parameter. In the present paper the approximation of fracture energy in phase field models is studied. Firstly, the diffusion equation of the phase field is numerically investigated. It is demonstrated through simple paradigmatic 2d and 3d cases that the fracture energy during crack initiation and propagation phenomena, such as crack branching and bifurcation, is strictly correlated with the internal length parameter. Moreover, it is shown that for finite value of the internal length parameter the dissipated energy does not depend only on the crack extension but on the geometrical configuration of fracture differently from the Griffith sharp approach. In particular, it is demonstrated that 3d cracks with same area may be characterized by different values of approximated fracture energy.

Keywords: variational fracture mechanics, phase field, damage, internal length scale, Gamma-convergence.

1. Introduction

The computational difficulties of discrete crack approaches to fracture can be overcome by the so called regularized models that have gained widespread popularity for simulating crack problems in a smeared manner. Among others, the phase field approach has demonstrated to be a very powerful analysis instrument. It derives from the variational theory of quasi-static crack evolution where the fracture problem solution is obtained as the minimization of energy functional constituted of a bulk term associated to the strain energy of the sound material and a surface contribution related to the fracture energy. The formulation is completed with irreversibility conditions for crack opening [1]. In [2], the free-discontinuity problem has been regularized with an elliptic two-field functional; the first field is classic and describes the macroscopic displacement in the body, whereas the other field can be physically interpreted as a damage variable which varies between 0 and 1, assumes the null value in the fractured zone and 1 far from it. For this reason it is also interpreted as a phase field. In this formulation the value of the stored energy functional is also affected by the spatial gradient of the phase field. The regularized functional is characterized by a parameter having the dimension of a length.

Huge efforts have been devoted to further enhance the phase field model in the scientific community. In fact, the original model proposed in [2] has been reformulated to prevent material overlapping and to reproduce more complex failure modes ([3, 4, 5, 6] and [7] for a review). More recently, the plastic material behavior has been analyzed in [8, 9, 10, 11, 12] to describe ductile fractures, and first attempts to reproduce the cohesive material response can be found in [13, 14]. Again, first trials to give a proper strategy for the evaluation of length scale parameter in accordance with experimental evidences have been proposed in [15, 16].

The mail goal of this study is to determine how the regularized formulation to fracture consistently approximates the Griffith theory of brittle fracture whenever the phase field approach represents a stand-alone modelling strategy. The fracture energy value that is dissipated during initiation and propagation of crack within a solid is correlated with the internal length scale parameter. In particular, the attention will be focused on the evaluation of the approximated fracture energy term of the regularized functional.

This work follows the line of recent papers that investigate specific aspects of the phase-field approach [17, 18, 19, 20], with the main focus to increase the potentiality of this computational instrument and thus to permit future consistent real world applications. Some of the previous points are resumed from literature and analysed with a different light others are totally new.

2. Formulation

The basic concepts of the phase field method are illustrated. The treatise covers only the minimum details that are instrumental for a clear comprehension of the paper.

2.1. Variational approach to fracture mechanics

Let $\Omega \in \mathbb{R}^d$ be a bounded open set with Lipschitz boundary representing the crack-free reference configuration of an elastic body. It is assumed that, due to proper external forces and boundary conditions, the body develops a $d-1$ dimensional crack and follows a displacement $\mathbf{u}$ out from the crack.

The strong formulation for a body characterized by brittle fracture is given by the following minimization problem

$$\min_{\mathbf{u}\in A} \Pi[\mathbf{u}], \quad A = \left\{\Gamma \subset \bar{\Omega}, \mathbf{u} \in C^1\left(\Omega \setminus \Gamma, \mathbb{R}^d\right) \,:\, \mathbf{u} = \bar{\mathbf{u}} \text{ on } \partial\Omega^{\mathcal{D}}\right\} \quad (1)$$

*Corresponding author
Email address: francesco.freddi@unipr.it (Francesco Freddi)

whit $\partial\Omega^{\mathcal{D}}$ the portion of $\partial\Omega$ with Dirichlet conditions $\mathbf{u} = \bar{\mathbf{u}}$ and the energy functional $\Pi[\mathbf{u}]$ is defined as

$$\Pi[\mathbf{u}] = \int_{\Omega\setminus\Gamma} \Psi(\nabla^s\mathbf{u})d\mathbf{x} \quad + \quad \gamma \,\text{meas}\,(\Gamma) \tag{2}$$

where Ψ is the strain energy density while the second term is a surface energy contribution *à la* Griffith where the constant γ represents the fracture energy, Γ is the fractured portion of the domain and "meas" is the $d-1$ Haussdorf measure. The strain energy density usually assumes the classical quadratic expression $\Psi = 1/2\mathbb{C}\,[\nabla^s\mathbf{u}]\cdot\nabla^s\mathbf{u}$ being $\mathbb{C}$ the fourth order elastic tensor of the sound material and $\nabla^s\mathbf{u}$ the symmetric part of the gradient $\nabla\mathbf{u}$. The formulation is completed by an irreversibility condition for fracture between two subsequent steps at time t and $t+\Delta t$: $\Gamma(t)\subseteq\Gamma(t+\triangle t)$ thus implying that crack length can only increase.

Alternatively, the present formulation can be rewritten on the subspace $SBD(\Omega)$ where the element Γ is replaced by $J_{\mathbf{u}}$ the set of jump points for $\mathbf{u}$ [21]. In the following, when Γ-convergence arguments are introduced it is intended meas (Γ) = meas $(J_{\mathbf{u}})$.

2.2. Regularization

To overcome the numerical difficulties of (1), a regularized strategy has been developed for the problem of sharp crack [2]. An additional field s describing the macroscopic damage (usually named phase field) is introduced. It represents the material state: for $s=1$ the solid is fully sound whereas $s=0$ indicates that cohesion is fully lost. The energetic contribution of fracture in (1) is approximated with the following expression:

$$\gamma\,\text{meas}(\Gamma) \sim \quad \frac{\gamma}{2}\int_\Omega l|\nabla s|^2 + \frac{(1-s)^2}{l}d\mathbf{x}\,, \tag{3}$$

where a second parameter l is introduced. This term can be interpreted as either a mathematical construction or an intrinsic material parameter.

Besides, the strain energy density of (2) is modified by an expression that depends both on the displacement vector $\mathbf{u}$, on the phase field s and vanishes in fully damaged zones: $\Psi(\nabla^s\mathbf{u}) \sim \Psi_s(\nabla^s\mathbf{u}, s)$. In the seminal work [2] it is assumed $\Psi_s(\nabla^s\mathbf{u}, s) = s^2\Psi(\nabla^s\mathbf{u})$. In [5] several expression of $\Psi_s(\nabla^s\mathbf{u}, s)$ are chosen in order to determine specific failure mechanics.

Indeed, in the phase field approach the energy functional (2) becomes

$$\Pi_l[\mathbf{u}, s] = \int_\Omega \Psi_s(\nabla^s\mathbf{u}, s)d\mathbf{x} \quad + \quad \frac{\gamma}{2}\int_\Omega l|\nabla s|^2 + \frac{(1-s)^2}{l}d\mathbf{x}\,. \tag{4}$$

The fracture problem (1) that involves both a volumetric and a superficial fracture term now is converted to the minimization, under proper boundary conditions, of functional (4) that presents only volumetric contributions

$$\begin{aligned} &\min_{\mathbf{u}\in\bar{A}} \Pi_l[\mathbf{u}, s],\ \bar{A} = \left\{(\mathbf{u}, s)\in W^{1,2}\left(\Omega, \mathbb{R}^d\right)\times W^{1,2}\left(\Omega, \mathbb{R}\right)\ :\ b.c.\right\}. \\ &b.c: \mathbf{u} = \bar{\mathbf{u}},\ s = 1 \text{ on } \partial\Omega^{\mathcal{D}}, \nabla s\cdot\mathbf{n} = 0 \text{ on } \partial\Omega\setminus\Omega^{\mathcal{D}} \end{aligned} \tag{5}$$

It has been proved in [22] that the approximated functional $\Pi_l[\mathbf{u}, s]$ Γ-converges to $\Pi[\mathbf{u}]$ for $l\to 0$. In addition, the evidences of Γ-convergence are valid for every single energy term of the functional [23]. In particular, for the energetic contribution associated to the phase field it results

$$\frac{\gamma}{2}\int_\Omega l|\nabla s|^2 + \frac{(1-s)^2}{l}d\mathbf{x} \underset{l\to 0}{\to} \gamma\,\text{meas}(\Gamma)\,. \tag{6}$$

Moreover, from functional (4) it is possible to derive the Euler-Lagrange equations, through variation with respect to the displacement and the phase field and imposing stationarity, that define the solid state:

$$\begin{cases} \text{div}\,\mathbf{T} = 0 \quad \text{in } \Omega \\ \frac{\gamma}{l}(s-1) - \gamma l\Delta s + \frac{\partial\Psi_s}{\partial s} = 0 \quad \text{in } \Omega\,, \end{cases} \tag{7}$$

where the body force has been neglected, $\mathbf{T}$ represents the Cauchy stress tensor and $\frac{\partial\Psi_s}{\partial s}$ is the driving force for damage that governs the failure mechanism within the solid. The system (7) is completed by the boundary conditions indicated in (5).

Then, in order to avoid material healing additional constraints on the evolution of the phase field are considered. The natural way to add such a constraint is to impose that $\dot{s}\le 0$. Alternative strategies have been introduced for computational convenience in [24] by considering the maximum value of the driving force during the load history. Differently, in [25] a threshold for the variable s is introduced to define the fully fractured regions; once that the threshold is overcome the irreversibility is imposed and the phase field is set $s=0$.

In finding the numerical solution, as well as to the discretization error of FEM, a second error has to be taken into account for a proper analysis of the results, as detailed in [25]. In fact, for linear finite elements discretization, the fracture energy has to be corrected by a factor that depends on h and l $\gamma\to\gamma\left(1+\frac{h}{2l}\right)$. This error is connected to the extra energy contribution within the finite elements that are fully damaged.

2.3. Fracture profile and length scale

The study of equations (7) in one dimension is a very simple and illuminating way to understand the impact of the regularization parameter l on the solution of the formulation. The elastic contribution is neglected and the solution is assumed to be stationary ($\dot{s}=0$). For fixed and small value of l, the damage $s(x)$ obtained under proper boundary conditions ($s(x_0)=0$, $s(\pm\infty)=1$) has the following profile

$$s(x) \sim 1 - e^{-\frac{|x-x_0|}{l}}, \tag{8}$$

for x close to point x_0 and $s\sim 1$ far away.

The smaller l gets, the higher gradients and curvatures of the solution $s(x)$ appears near the crack at $x=x_0$. The limit $l\to 0$ yields a discontinuous function, which is 0 at $x=x_0$ and 1 elsewhere. In case the optimal profile (8) is adopted, the integral (3) gives a result that does not depend on the parameter l; the approximated fracture energy is equivalent to the one expected for sharp crack.

The damage energy density (3) could be replaced, in a more complex model, by general terms of the form $lf(\nabla s)+g(1-s)/l$, with the limitation on $f(\cdot)$ and $g(\cdot)$ to be positive convex functions null at the origin. The profile of the phase field variable

s will depend on the specific choice of f and g, determining a different behavior of the damaged zones. In any case, the width of the damaged portion would still be of the order l. Here, we just consider the energy (3); different choices for f, for example $(1-s)/l$, would lead to similar numerical results.

3. Numerical simulations

In this section several simulations are presented. Firstly, some simple cases are devoted to the evaluation of the fracture energy and successively the initiation and evolution of rupture is investigated. Numerical details concerning the solution strategy can be found in [5], [17]. In the proposed tests irreversibility is imposed by considering the strategy proposed in [19]. In such a way the condition does not affect the phase field profile [20]. The numerical simulations have been conducted with a specific code based upon the Open Source package deal.II [26].

3.1. Fracture energy estimation

The attention is focused on the proper evaluation of the fracture energy contribution in simple paradigmatic cases in 2 and 3 dimensions. In these numerical simulations the domain Ω comes with a fracture Γ whereas mechanical effects are neglected. Accordingly, the phase-field equation of the system (7) reads

$$(s-1) - l^2 \Delta s = 0 \quad \text{in } \Omega\,. \tag{9}$$

On the external boundary $\partial\Omega$ the Neumann condition $\nabla s \cdot \mathbf{n} = 0$ is imposed whereas on the fractured portion Γ of the solid $s = 0$ is set. This case is the natural extension in 2d or 3d setup of the 1d problem that gives rise to the optimal profile expression (8). Now, the solution is determined numerically.

Once that equation (9) has been numerically solved via FEM, the approximated fracture energy $\Phi[\Gamma_l]$ is computed with the expression

$$\Phi[\Gamma_l] = \frac{\gamma}{2} \int_\Omega l|\nabla s|^2 + \frac{(1-s)^2}{l}\, d\mathbf{x}\,. \tag{10}$$

where Γ_l is defined as the crack representation in the regularized formulation and it has dimension $d-1$. In these examples, because the solid is already fractured $\Gamma_l \equiv \Gamma$, otherwise in computations where crack propagates a careful treatment permits to determine Γ_l as detailed in the simulation described in Section 3.2. For simplicity, in all the simulations $\gamma = 1$ has been assumed .

3.1.1. 2D fracture

Firstly, a simple unitary square continuum in 2 dimensions with a sharp crack surface is considered. Two cases have been considered in order to numerically assess the solution strategy: a fully developed crack from side to side illustrated in Fig. 1a and a sharp fracture from the left side to the center as indicated in Fig. 1b.

A uniform regular mesh is employed for the discretization. In particular, bilinear quadrilateral lagrangian finite elements have been considered. For different values of the internal length scale parameter $l \in \{0.05, 0.025, 0.0125, 0.00625\}$, the stationary solution of the evolution equation of damage (9) was computed with different meshes ranging from 4000 (20x20) to 409600 (640x640) elements. Once the solution of (9) has been calculated the value of the regularized fracture energy is computed through eq. (10). The aim of this investigation is to rule out the discretization error.

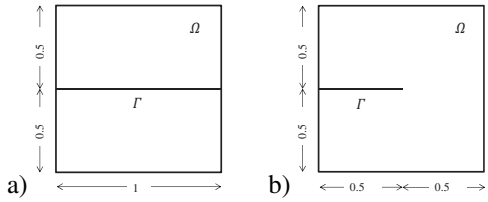

Figure 1: Square domain with a sharp crack a) full b) half.

In Fig. 2b the relative error is plotted as a function of the dofs for the four values of l. The smaller is the parameter l the bigger is the numerical error. This fact is due to the higher gradient in the s profile that becomes sharper as l diminishes. In all cases linear slope is evidenced in the bi-log plots. It may be concluded that the numerical simulation correctly estimates the expected value of fracture energy.

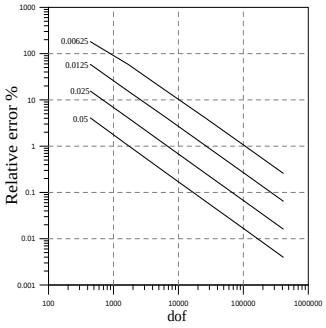

Figure 2: Fully developed crack: surface energy error as a function of the dof for different values of the parameter l.

In Table 1 the value of the fracture energy (10) is reported for 409600 elements. Here, the error, only due to FEM discretization that is fixed, grows slightly as l diminishes. The use of finer meshes as l decreases would lead to constant error.

It can be concluded that in this case the approximated fracture energy gives the Griffith fracture energy whatever is the value of l so that

$$\Phi[\Gamma_l] \approx \text{meas}(\Gamma)\,. \tag{11}$$

and the phase field solution in a direction orthogonal to the fractured surface Γ_l always assumes the optimal profile behavior (recalling the Remark on the optimal profile). Obviously, relation (11) is worth only if the numerical approximation error is small.

l	Full crack $\Phi[\Gamma_l]$	Half crack $\Phi[\Gamma_l]$	L-shape $\Phi[\Gamma_l]$	T-shape $\Phi[\Gamma_l]$
0.05	1.00004	0.525165	0.983243	1.43642
0.025	1.00016	0.512681	0.991816	1.46841
0.0125	1.00065	0.506493	0.995990	1.48505
0.00625	1.00260	0.503614	0.998581	1.49592
sharp fracture energy	1.0	0.5	1.0	1.5
α of (12)	0	0.5	-1/3	-4/3

Table 1: Values of the approximated fracture energy $\Phi[\Gamma_l]$ obtained for different values of l in the four 2D cases illustrated in Figs. 1, 5 adopting a uniform mesh with 409600 elements. The value for the Griffith theory is reported. In the last row the expected value for coefficient α of (12) is indicated.

The same analysis has been conducted for the case of a sharp half side crack of Fig. 1b. Now, the convergence results illustrated in Figs. 3 are no more linear and high precision cannot be achieved even if a very fine mesh is adopted. Indeed, the error asymptotically converges to a fixed value whatever is the value of l.

The obtained measures of $\Phi[\Gamma_l]$ are reported in Table 1 for different values of the internal length scale. The fracture energy approximation approaches 0.5 for smaller value of l in accordance with Γ-convergence result (6). Other expressions of the regularized fracture energy lead to similar results as outlined by the Γ-convergence numerical test reported in Section 5.1 of [27]. However one would expect, as in the previous case that the higher is the gradient of the solution the bigger is the error in the evaluation of the fracture energy contribution.

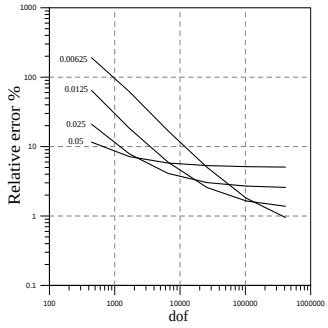

Figure 3: Half crack: approximated fracture energy error as a function of the dof for different values of the parameter l.

Therefore, the problem is deeply investigated by fixing the attention on the case $l = 0.0125$ mm. In Fig. 4a the map of the phase field solution is plotted. The solution is affected by the presence of the crack tip. Then, the behavior of the phase field is extrapolated from the FEM results along three directions 1, 2 and 3 as indicated in Fig. 4a. In details, two numerical solutions are plotted starting from the crack tip along two orthogonal directions (1 and 2) whereas the remaining damage profile is calculated orthogonally to the crack far from the tip (3). Fig. 4b compares the computed phase field values with the optimal profile of (8). Along the direction 3 the numerical solution captures the analytical profile perfectly, whereas the damage plots starting from the crack tip differ from the phase field profile of (8) along both the directions. This evidence reveals that the numerical solution obtained in the vicinity of the crack tip presents a graph that is similar to the optimal profile of (8) but with a sharper behavior.

So, the numerical convergence at fixed l leads to unexpected value of the fracture energy (different from the sharp fracture energy 0.5). In fact, a careful numerical investigation has permitted to determine a tentative expression of the expected value for the case at hand that can be written as

$$\Phi[\Gamma_l] \cong \gamma \cdot \mathrm{meas}(\Gamma_l) + \gamma l \alpha \,, \tag{12}$$

where a term associated to the crack tip is introduced. Such term depends linearly on the parameter l, on the fracture energy γ and on a coefficient α. For the analysed case the numerical results suggest for α the value 0.5. Besides, the second term of (12) vanishes as $l \to 0$ according to the $\Gamma-$convergence results.

In Fig. 4c the relative error between the value of fracture energy obtained from the r.h.s. of (12) and that achieved from the numerical solutions previously plotted in Fig. 3 is redrawn. The linear convergence evidenced for the case of a fully developed crack (illustrated in Fig. 2b) is almost restored thus revealing that the r.h.s. of expression (12) represents a good approximation of the approximated fracture energy. The approximation could be improved by considering higher order terms in (12).

Therefore, for finite values of l, the approximated fracture energy overestimates the Griffith energy, thanks to the additional diffusion contribution around the crack tip which completely lacks in sharp representation of crack.

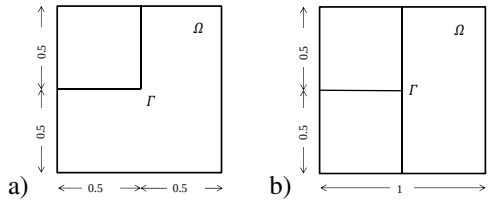

Figure 5: Square domain with a sharp crack a) L-shape b) T-shape.

Successively, two additional configurations have been investigated. The first one is reported in Fig. 5a and is representative of a kinked crack, whereas the second case, that simulates fracture bifurcation, is depicted in Fig. 5b. The results are listed in Table 1. In both cases, the expected fracture energy value is underestimated; an additional term similar to the one reported in (12) is confirmed. Here, the solution in the proximity of the kinking point presents a diffusion that again differs from the optimal profile.

For these two examples the value of the coefficient α of (12) has been estimated and reported in the last row of Table 1: in both cases it is a negative value. Now, the approximated fracture energy $\Phi[\Gamma_l]$ underestimates the energy of sharp fracture because of the reduced diffusion of damage near the corners.

Infinite geometrical configurations can be tested in these two last examples: different kinking and bifurcation angles and length ratio between the crack branches. The analysis of all these geometries is out of the aim of this work. Attention has been limited to simple cases that promise high numerical precision and are free of the anisotropy error induced by mesh orientation, so that convergence can be achieved. However, parametric analysis could be performed for specific cases.

3.1.2. 3D fracture

Similar tests have been performed even in 3d configurations. Computations have been conducted on a cubic domain with unitary side. Three cases have been analysed: a fully developed crack, an edge fracture and an inner fracture as illustrated in Fig. 6. For these numerical simulations, uniform discretizations composed by hexahedral linear finite elements have been adopted. The approximated values of the fracture energy are reported in Table 2.

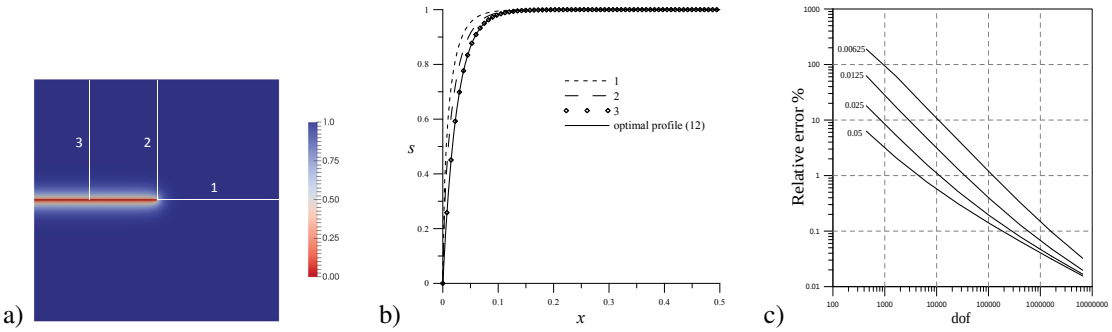

Figure 4: Half crack: a) 2D map of the phase field, b) Comparison of the computed 2D phase field to 1D optimal profile of (8) along the three directions indicated in Fig. 4a, c) corrected approximated fracture energy error as a function of the dof for different values of l.

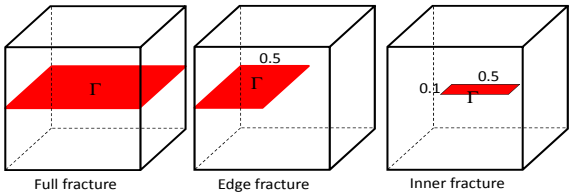

Figure 6: 3D tests: cube with different fracture configurations.

As in 2d for a fully developed crack that crosses the entire body, the solution exactly converges to the one obtainable from the Griffith theory: the error, only due to the discretization, grows as l decreases as outlined in Table 2. The phase field solution in a direction orthogonal to the fractured surface Γ always assumes the optimal profile behavior.

In the second example of an edge crack that involves half of the domain thickness, the crack front is almost completely inside the solid, in a configuration similar to the one illustrated in the 2d case of a half crack. The data reported in Table 2 are equivalent to the results of Table 1. Also here an additional contribution, associated to the crack tip, modifies the value of the approximated fracture energy. Even the third dimension influences the result and the second term at r.h.s. of (12) has to be multiplied by the front length that here is 1.

Finally, a small internal rupture with a surface equal to 0.05 mm^2 is considered. Now, the whole crack front of the fracture is within the solid. This case is representative of a crack that nucleates at the interior of the domain. The values of the approximated fracture energy reported in Table 2 differ significantly from the ones obtainable from the Griffith theory. As in the previous cases, the difference decreases as $l \to 0$ according to the Γ-convergence results of (6).

l	Full crack $\Phi[\Gamma_l]$	Edge crack $\Phi[\Gamma_l]$	Inner crack $\Phi[\Gamma_l]$	Inner crack $\Phi[\Gamma_l]$ (13)
0.05	1.00004	0.525165	0.0811488	0.08
0.025	1.00016	0.512681	0.0657384	0.065
0.0125	1.00065	0.506493	0.0580888	0.0575
0.00625	1.00260	0.503614	0.0543264	0.05375
sharp fracture energy	1.0	0.5	0.05	0.05

Table 2: Values of the approximated fracture energy $\Phi[\Gamma_l]$ obtained for different values of l in the 3D cases of a complete, half and inner fracture. In the last row the expected value for the Griffith theory is reported. The last column indicates the expected value of the approximated fracture energy according to (13).

For the last example, the approximated expression of the fracture energy (12) is modified in order to consider the additional contributions due to the crack front length and the four corners

$$\Phi[\Gamma_l] \cong \gamma \cdot \text{meas}(\Gamma_l) + \gamma l \alpha \cdot \text{meas}(\partial\Gamma_l) + \text{Effect of corners}\,. \qquad (13)$$

Also in this case it results $\alpha = 0.5$. The evaluation of the last term, associated to the four corners of the fracture surface, is extremely complicated and it plays a minor role with respect to the one associated to the crack front measure. In fact, the last column of Table 2 reports the expected values of the approximated fracture energy in accordance with (13) neglecting the last term due to corners. The difference between these approximated values and those obtained from FEM computations is rather limited. The results are in accordance with (13) and exacerbate the importance of the additional term associated to the crack front.

3.2. *Complete problem*

Now, the complete problem (7) is studied through a simple example. It simulates a double cantilever beam in bending and is characterized by stable crack propagation after nucleation. The test case is solved at a practical length scale thus permitting to investigate the behavior of the model in reproducing real experiments. The dimensions of the domain are two orders of magnitude greater than l and the mesh resolution is reasonably coarse for competitive computation costs. Such assumptions are common and widely adopted in the scientific community. The crack propagation is stable as the displacement is applied on the boundary as shown in Fig. 7.

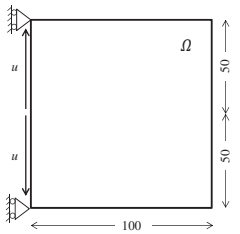

Figure 7: Double cantilever beam problem: geometry and boundary conditions.

The material properties assumed for the analysis are E=100 MPa, ν=0.25, γ=0.01 N/mm, l=1 mm. Plane strain and quasi-static hypotheses are assumed. The solid is discretized with

34624 quadrilateral bilinear elements. The mesh is non-uniform with smaller elements in the central portion of the domain such that $h \approx 0.25l$. Differently from [28] no initial flaw is artificially imposed by Dirichlet boundary conditions for s. For symmetry reason, the damage process develops at the middle of the left vertical side and propagates horizontally.

Aims of this example are: comparing the energy of the approximated model with the ideal one of sharp brittle fracture during the propagation process and analysing the fracture energy increment.

Understanding the effective critical energy release rate is decisive when explaining numerical results, because it determines if the model over- or under-estimates fracture evolution. For this purpose, the effective critical energy release rate is defined as

$$\gamma_{\text{eff}} = \frac{\Phi[\Gamma_l]}{\text{meas}(\Gamma_l)}$$

the ratio between the approximated fracture energy $\Phi[\Gamma_l]$ and the fracture length $\text{meas}(\Gamma_l)$.

One of the difficulties associated with phase-field models for fracture is defining the crack tip location in order to evaluate the term $\text{meas}(\Gamma_l)$ which represents the length of the smeared fracture. In these computations, the phase-field value $s = 0.2$ as adopted in [28] determines the tip position. Furthermore, a comparison is made by assuming the tip located at $s = 0.05$.

In Fig. 8 the ratio $\gamma_{\text{eff}}/\gamma$, that measures the distance of the smeared approach towards a pure brittle fracture, is reported as a function of the crack length $\text{meas}(\Gamma_l)$. For short crack the difference is evident. The regularized model presents higher energetic values with respect to the sharp approach. In fact, the pristine state necessitates first that damage initiates and diffuses before fracture starts propagating. This process is totally absent in the Griffith theory that requires an initial defect. Moreover, the crack presents a tip within the solid; thus, the smeared approach overestimates the dissipated energy at the initiation stage and for very short fracture.

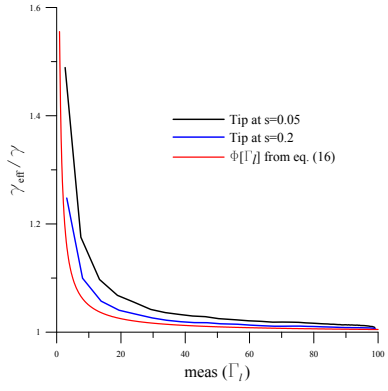

Figure 8: Double cantilever beam problem: $\gamma_{\text{eff}}/\gamma$ as a function of the crack length.

In [29] authors noticed an overestimation of the critical load in undamaged notch conditions. The result illustrated here confirms, as stated in [19], the need to overcome and energetic barrier associated with bifurcation from an undamaged state to a fully broken state.

As the crack propagates the ratio $\gamma_{\text{eff}}/\gamma \to 1$. The difference between the two adopted crack tip positions is remarkable only for very short fracture. The regularized approach always overestimates the sharp energy even at complete fractured solid. This fact is due to the numerical error induced by the discretization that cannot be completely removed as also outlined in [28]. In the same Figure it has been also reported the value of γ_{eff} obtained by (12). The behavior confirms the numerical solutions even if lower energetic values are indicated. This is probably due to the fact that (12) is an approximated expression obtained for an ideal crack, neglecting the driving force effect or other more complex phenomena that cannot be estimated. Further error is due to uncertain location of the crack tip and, consequently, on the value of $\text{meas}(\Gamma_l)$.

Consider now two subsequent time steps at time t and $t + \Delta t$: the change in surface energy associated to the crack length variation is $\Delta\Phi[\Gamma_l] = \Phi[\Gamma_l](t + \Delta t) - \Phi[\Gamma_l](t)$. The energy spent in fracture propagation is reported in Table 3 at different crack lengths associated to a displacement increment Δu.

$\text{meas}(\Gamma_l)$	$\text{meas}(\Delta\Gamma_l)$	$\Delta\Phi[\Gamma_l]$	$\gamma_{\text{eff}} = \frac{\Delta\Phi[\Gamma_l]}{\text{meas}(\Delta\Gamma_l)}$
3.1497	4.9095	0.04944	0.01007
29.722	4.510	0.04492	0.009961
60.244	3.885	0.03873	0.009970

Table 3: γ_{eff} during the propagation phase associated to an increment length $\text{meas}(\Delta\Gamma_l)$.

The obtained value of γ_{eff} is always very precise regardless the position of the crack and its length. This means that the extremely regular crack propagation is energetically described as a pure Griffith type fracture. In this test, the discrepancy between the sharp and smeared approaches is only associated to the initiation stage of fracture and by the presence of the crack tip.

The crack initiates at the middle of the left vertical side and propagates horizontally. The onset of fracture presents a very small fully damaged region which is representative of the crack tip development. The energetic difference between the smeared and the sharp approach is exacerbated at this stage: in the approximated approach the energy associated to this phenomenon is not null whereas it cannot be captured by the Griffith theory of fracture that here highlights the need of pre-existing flaw within the solid. Instead, the crack growth is only associated to a fracture extension associated to a tip motion and in this step the two approaches are energetically equivalent.

4. Discussion of the results

In summary, a tentative first order approximation of smeared fracture energy is

$$\Phi[\Gamma_l] \cong \gamma \cdot \text{meas}(\Gamma_l) + \gamma\, l\, F(\text{geometry}, \text{topology})\,. \qquad (14)$$

This formula can be seen as a generalization of (12) where the value of $\Phi[\Gamma_l]$ is obtained as the sum of two contributions: the measure of Γ_l in a Griffith sense and a term that depends upon the coefficient γ, the internal length l and a function F representative of the geometry of the damaged zones. The consequences of (14) can be different.

In 2d setup the additional term associated to the geometry can be predominant at the nucleation stage, for short crack or in case of interaction between fractures. Otherwise, for long crack it results $l/\text{meas}(\Gamma_l) \to 0$ thus the difference between the approximated fracture energy and the value of the sharp theory vanishes in accordance with the Γ-convergence results, as clearly outlined by the test case of a double cantilever beam.

In 3d configuration the situation is much more intricate. In fact, inner crack can give extremely variable value of fracture energy, as evidenced from numerical simulations. A simple example will permit to appreciate the intrinsic meaning of (14).

Let us consider two simple cracks with the same area in an infinite domain: the first one has a circular front with radius a whereas the other has an elliptic shape with semi-axis $n\,a$ and a/n with $n \in \mathbb{R}^+$. Now eq. (12) reduces to

$$\Phi[\Gamma_l] \cong \gamma \cdot \text{meas}(\Gamma_l) + \gamma\, l\alpha \cdot \text{meas}(\partial\Gamma_l)\,, \tag{15}$$

where the additional terms associated to the crack front length of (15) are $\pi a\, l$ and $0.5 l\pi \left[3\,(na + a/n) - \sqrt{3\,(na + a/n)\,(na + 3a/n)}\right]$ for the circular and elliptical[1] fracture respectively and α is equal to 0.5.

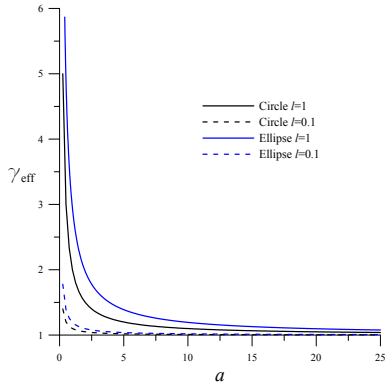

Figure 9: Expected γ_{eff} for the approximated fracture energy in case of a 3D inner fracture with circular or elliptic front as a function of the dimension a.

The specific cases with $n = 3$, $\gamma = 1$ and $l \in 0.1, 1$ mm are analysed. According to (15), two cracks with the same area have different values of approximated fracture energy; this is only due to the different crack shape and front length. In Fig. 9 the value of γ_{eff} obtained from the approximated fracture energy according to (15) is plotted for two values of l as a function of the fracture dimension a. For graphical reason the curves have been truncated because $\gamma_{\text{eff}} \to \infty$ as $a \to 0$. The behavior of γ_{eff} is similar to the result of the 2d example previously modelled and depicted in Fig. 7b. For $l = 0.1$ mm and high values of a it results $\gamma_{\text{eff}} \to \gamma$; the difference in term of energy between the two surfaces is rather limited. At the crack onset as $a \to 0$, the value of γ_{eff} assumes value greater than γ especially for the case of elliptic fracture. This phenomenon is much more evident for $l = 1$ mm; for small fracture extension γ_{eff} explodes (as clearly illustrated in Fig. 9b). The greater is l, the higher the difference between the sharp and the regularized representation of fracture is. Moreover, the energetic difference between the two fractures, circular and elliptical, is evident and it is still present for large values of a. The circular fracture with a shorter front better approximates the energy of sharp fracture whereas the elliptic one, with a longer crack front, presents higher energetic values.

[1] This approximated expression due to Ramanujan of the ellipse perimeter is valid for $n > 1$. Even if exact formulas based on infinite series are available the adopted expression permits to get a very good precision for the example.

5. Conclusions

This work provides a critical numerical estimation of the approximated fracture energy calculated in the phase-field model for brittle fracture of the original formulation proposed in [2]. It has been shown that the regularized approach offers a solution that can be understood richer than the one obtainable from a model fully based on the Griffith's theory.

Specifically, the simulations have shown that when the fracture involves the whole section of the solid the approximated value of the fracture energy does not depend on the internal length scale parameter. In all the other cases, the approximated value of the fracture energy is influenced by the geometry of the crack, its onset and propagation stages. In particular, for finite value of l, the smeared fracture energy differs from the one predicted by Griffith's theory. As shown, the phase field distribution abandons the optimal profile in the proximity of the crack tip or front, at kinking and bifurcation points among the infinite scenarios. Moreover, the interaction between adjacent but distinct cracks would certainly modify the process zone.

In conclusion, the smaller l is with respect to both the crack length and the specimen geometry, the closer the phase-field strategy approaches the ideal Griffith result; the small scale process zone assumption is valid.

Again, in 3d setup the situation is even more intricate because fractures with same area but dissimilar crack front length may considerably differ from the energetic point of view. It is still an open problem the initiation of an inner fracture in 3d solid.

Moreover, it has been quantified the difference between the sharp and regularized fracture approaches. In particular, the strategies give equivalent results for vanishing internal length. For finite value l plays a non-negligible contribution. It defines the width of the process zone and implicitly introduces a structural factor that is directly correlated to the material parameter l. It may be concluded that two parameters, one associated to the strength of the material and an internal length scale, are crucial for the analysis of fracture process characterized by diffusive phenomena. Analogous conclusion was given in [30] where - starting from the experimental evidences that have shown how crack initiation at corners, V-notches and other situations such as interfaces breaking a free surface (delamination initiation) cannot be correctly predicted by the usual brittle fracture criteria (either Griffith or maximum stress) - a fracture onset criterion based on two parameters has been proposed: a toughness (in general a characteristic energy) and a characteristic length (that is not only a material parameter but a structural one de-

pending for example on the notch opening thus enclosing the diffusion of damage within the solid).

References

[1] G. A. Francfort, J.-J. Marigo, Revisiting brittle fracture as an energy minimization problem, J. Mech. Phys. Solids 46 (1998) 1319–1342.

[2] B. Bourdin, G. A. Francfort, J.-J. Marigo, Numerical experiments in revisited brittle fracture, J. Mech. Phys. Solids 48 (2000) 797–826.

[3] H. Amor, J.-J. Marigo, C. Maurini, Regularized formulation of the variational brittle fracture with unilateral contact: Numerical experiments, Journal of the Mechanics and Physics of Solids 57 (2009) 1209 – 1229.

[4] G. Lancioni, G. Royer-Carfagni, The variational approach to fracture mechanics. a practical application to the french panthéon in paris, Journal of Elasticity 95 (2009) 1–30.

[5] F. Freddi, G. Royer-Carfagni, Regularized variational theories of fracture: A unified approach, Journal of the Mechanics and Physics of Solids 58 (2010) 1154 – 1174.

[6] F. Freddi, G. Royer-Carfagni, Variational fracture mechanics to model compressive splitting of masonry-like materials, Annals of Solid and Structural Mechanics 2 (2011) 57–67.

[7] M. Ambati, T. Gerasimov, L. De Lorenzis, A review on phase-field models of brittle fracture and a new fast hybrid formulation, Computational Mechanics 55 (2015) 383–405.

[8] F. Freddi, G. Royer-Carfagni, Plastic Flow as an Energy Minimization Problem. Numerical Experiments, Journal of Elasticity 116 (2014) 53–74.

[9] R. Alessi, J.-J. Marigo, S. Vidoli, Gradient damage models coupled with plasticity: Variational formulation and main properties, Mechanics of Materials 80 (2015) 351–367.

[10] F. Freddi, G. Royer-Carfagni, Phase-field slip-line theory of plasticity, Journal of the Mechanics and Physics of Solids 94 (2016) 257–272.

[11] R. Alessi, J.-J. Marigo, C. Maurini, S. Vidoli, Coupling damage and plasticity for a phase-field regularisation of brittle, cohesive and ductile fracture: One-dimensional examples, International Journal of Mechanical Sciences (2017).

[12] J. Choo, W. Sun, Coupled phase-field and plasticity modeling of geological materials: From brittle fracture to ductile flow, Computer Methods in Applied Mechanics and Engineering 330 (2018) 1 – 32.

[13] S. May, J. Vignollet, R. de Borst, A numerical assessment of phase-field models for brittle and cohesive fracture: γ-convergence and stress oscillations, European Journal of Mechanics - A/Solids 52 (2015) 72 – 84.

[14] F. Freddi, F. Iurlano, Numerical insight of a variational smeared approach to cohesive fracture, Journal of the Mechanics and Physics of Solids 98 (2017) 156–171.

[15] T. T. Nguyen, J. Yvonnet, M. Bornert, C. Chateau, K. Sab, R. Romani, R. Le Roy, On the choice of parameters in the phase field method for simulating crack initiation with experimental validation, International Journal of Fracture 197 (2016) 213–226.

[16] X. Zhang, C. Vignes, S. W. Sloan, D. Sheng, Numerical evaluation of the phase-field model for brittle fracture with emphasis on the length scale, Computational Mechanics 59 (2017) 737–752.

[17] A. Mesgarnejad, B. Bourdin, M. Khonsari, Validation simulations for the variational approach to fracture, Computer Methods in Applied Mechanics and Engineering 290 (2015) 420–437.

[18] K. H. Pham, K. Ravi-Chandar, C. M. Landis, Experimental validation of a phase-field model for fracture, International Journal of Fracture 205 (2017) 83–101.

[19] E. Tann, T. Li, B. Bourdin, J.-J. Marigo, C. Maurini, Crack nucleation in variational phase-field models of brittle fracture, Journal of the Mechanics and Physics of Solids 110 (2018) 80 – 99.

[20] T. Linse, P. Hennig, M. Kastner, R. de Borst, A convergence study of phase-field models for brittle fracture, Engineering Fracture Mechanics 184 (2017) 307 – 318.

[21] S. Conti, M. Focardi, F. Iurlano, Which special functions of bounded deformation have bounded variation?, Preprint arXiv:1502.07464 (2015).

[22] L. Ambrosio, V. M. Tortorelli, On the approximation of free discontinuity problems, Boll. Un. Mat. Ital. B (7) 6 (1992) 105–123.

[23] F. Iurlano, A density result for GSBD and its application to the approximation of brittle fracture energies, Calc. Var. Partial Differential Equations 51 (2014) 315–342.

[24] C. Miehe, F. Welschinger, M. Hofacker, Thermodynamically consistent phase-field models of fracture: Variational principles and multi-field fe implementations, International Journal for Numerical Methods in Engineering 83 (2010) 1273–1311.

[25] B. Bourdin, G. A. Francfort, J.-J. Marigo, The variational approach to fracture, J. Elasticity 91 (2008) 5–148.

[26] W. Bangerth, R. Hartmann, G. Kanschat, deal.II – a general purpose object oriented finite element library, ACM Trans. Math. Softw. 33 (2007) 24/1–24/27.

[27] J.-Y. Wu, A unified phase-field theory for the mechanics of damage and quasi-brittle failure, Journal of the Mechanics and Physics of Solids 103 (2017) 72 – 99.

[28] M. J. Borden, T. J. Hughes, C. M. Landis, C. V. Verhoosel, A higher-order phase-field model for brittle fracture: Formulation and analysis within the isogeometric analysis framework, Computer Methods in Applied Mechanics and Engineering 273 (2014) 100 – 118.

[29] M. Klinsmann, D. Rosato, M. Kamlah, R. M. McMeeking, An assessment of the phase field formulation for crack growth, Computer Methods in Applied Mechanics and Engineering 294 (2015) 313 – 330.

[30] D. Leguillon, Strength or toughness? a criterion for crack onset at a notch, European Journal of Mechanics - A/Solids 21 (2002) 61 – 72.